Dual Effect of Anionic Surfactants in the Electrodeposited MnO_2 Trafficking Redox Ions for Energy Storage

Avijit Biswal,[a,b,c] Bankim Chandra Tripathy,[a,b] Tondepu Subbaiah,[a,b] Danielle Meyrick,[c] and Manickam Minakshi[c,z]

[a]*CSIR, Institute of Minerals and Materials Technology, Bhubaneswar, 751013 Odisha, India*
[b]*Academy of Scientific and Innovative Research, Training and Development Complex, Chennai 600 113, India*
[c]*School of Engineering and Information Technology, Murdoch University, Murdoch, WA 6150, Australia*

The dual effect of in-situ addition of anionic surfactants, sodium octyl sulfate (SOS), sodium dodecyl sulfate (SDS) and sodium tetradecyl sulfate (STS) on the microstructure and electrochemical properties of electrolytic manganese dioxide (EMD) produced from waste low grade manganese residue is discussed. X-ray diffraction (XRD), field emission scanning electron microscopy (FESEM), BET-surface area studies, thermogravimetry-differential thermal analysis (TG-DTA) and Fourier transform infrared spectroscopy (FTIR) were used to determine the structure and chemistry of the EMD. All EMD samples were found to contain predominantly γ-phase MnO_2, which is electrochemically active for energy storage applications. FESEM images showed that needle, rod and flower shaped nano-particles with a porous surface and platy nano-particles were obtained in the case of EMD deposited with and without surfactant respectively. Thermal studies showed loss of structural water and formation of lower manganese oxides indicating high stability of the EMD samples. The cyclic voltammetry and charge – discharge characteristics implied the presence of surfactants enhances the energy storage within the MnO_2 structure. Addition of the surfactant at its optimum concentration greatly increased the EMD surface area, which in turn improved the cycle life of the EMD cathode. EMD obtained in the presence of 25, 50, 25 ppm of SOS, SDS, and STS respectively showed an improved cycle life relative to the EMD obtained in the absence of surfactant. EMD obtained without surfactant showed a capacity fade of 20 mAh g^{-1} within 15 discharge-charge cycles, while surfactant modified samples showed stable cyclic behavior of capacity 95 mAh g^{-1} even after 15 cycles.
 [DOI: 10.1149/2.0191501jes]

Manuscript submitted August 15, 2014; revised manuscript received October 21, 2014. Published November 8, 2014.

Global demand for new energy materials and energy storage devices is increasing rapidly and in parallel with the quest for alternative energy resources. Substantial research and development effort continues to be invested in the synthesis of an economically viable, ecofriendly storage device from a natural source. Among the various energy storage devices, alkaline rechargeable batteries have become the ultimate choice for energy storage systems in the portable electronics market as well as electric transport systems.[1–3] Worldwide research and development programs in this area have been underway for more than a century,[2] with most attention focused on Zn-Mn, Ni-Cd, Ni-Fe, Ni-Zn, Ni-MH, and Li-ion rechargeable systems.[4] Among these, Zn-Mn alkaline batteries have held a strong position in the battery market for many decades.

Manganese dioxide, used as the active material in Zn-MnO_2 batteries, can be prepared both by chemical synthesis (chemical manganese dioxide, CMD) or electrochemical deposition (electrodeposited manganese dioxide, EMD) methods. Adequate primary Mn resources are available from which manganese dioxide can be produced, but the rapidly growing demand for manganese/manganese oxide has made it increasingly important to develop processes for economic recovery of manganese from low-grade manganese ores and other sources.[5] In order to fulfill the escalating demand of EMD for its application in rechargeable batteries and super capacitors, production of EMD from secondary resources is of great importance.

Polymetallic nodules are a rich source of many metals, and exploration of manganese nodules has been carried out at various locations around the world for a number of decades. Mn leach residue and Mn cake are two waste products obtained during the extraction of Cu, Ni, Co, and Zn. Battery grade EMD has been successfully prepared from Mn cake.[6,7] Attempt has also been made to prepare battery grade EMD from manganese sulfate solution obtained from Mn leach residue[8] which is a waste material obtained during the processing of Mn nodules.[9] The present authors have also compared the suitability of EMDs obtained from manganese cake, leach residue and synthetic solution as battery materials and found that EMDs obtained from secondary sources gave better performance over the synthetic one.[10]

[z]E-mail: minakshi@murdoch.edu.au

Purity and quality are two important factors governing the electrochemical activity of EMD. EMD as electroactive material has found applications in primary as well as rechargeable alkaline batteries due to the purity of the predominantly γ-phase MnO_2. Although its use in alkaline batteries dates back about 40 years, there remains a technology drive to improve its rechargeability.[11–16] Low production cost, low environmental impact, high redox potential, high rate capability, better relative performance over a wide temperature range, and long storage life[15,17–19] are distinct features of pure EMD. In improving the quality of EMD, surfactants play a role by modifying the microstructure, which in turn affects the electrochemical activity of the EMD. Although use of surfactants during electrodeposition may not be new, their use during production of EMD, and consequent effect on EMD structure and performance, remains to be fully explored. It has also been demonstrated that surfactants can play a role in promoting crystal growth and aggregation, facilitating the efficient transport of redox ions, a prerequisite for any energy storage material such as EMD.

Surfactants are commonly used in the preparation of various electrode materials by a number of different techniques, such as chemical co-precipitation[20,21] and liquid co-precipitation,[22] in addition to electrochemical deposition methods.[23,24] Ghaemi et al.[24] have reported that electrolytic MnO_2 prepared in the laboratory in the absence of surfactant does not have properties appropriate for battery applications. On the other hand, the electrochemical behavior of EMD prepared in the presence of surfactants—namely, t-octyl phenoxy polyethoxyethanol (Triton X-100), cetyltrimethylammonium bromide (CTAB), or sodium n-dodecylbenzenesulfonate (SDBS)—is suitable for battery applications.[25] The effect of quaternary amines on the electrochemical behavior of EMD was discussed in our previous work.[26] Recent literature[27,28] reports the effect of sodium dodecyl sulfate (SDS) on the supercapacitive behavior of EMD. For the first time, we reported in our recent work[29] the K intercalation behavior of EMD modified by Triton X-100. Due to the rising demand for EMD, continual efforts are underway to find alternative sources from which EMD can be produced with better electrochemical performance.

The present work reports the performance and properties of EMD produced from low grade manganese leach residue in the presence of anionic surfactants sodium octyl sulfate (SOS), sodium dodecyl sulfate (SDS) and sodium tetradecyl sulfate (STS). Mn leach residue is

obtained during ammoniacal leaching of manganese nodule,[10] and is usually considered as waste and discarded. Surfactants possess a long chain hydrophobic group attached to a hydrophilic head group, which can adsorb on the electrode surface and influence the mechanism of redox processes. Ionic surfactants in aqueous solution may be classified as cationic or anionic; the sodium salts of higher fatty acids such as SOS, SDS, and STS are classed as anionic surfactants. The critical micelle concentrations (CMC) of the surfactants[30,31] SOS, SDS, and STS are 133, 8 and 2 mM, respectively. The aim of the present study is to investigate the influence of three different anionic surfactants and their dual role on materials and electrochemical properties.

Experimental

Materials and methods for producing EMD.— Electrolytic manganese dioxide (EMD) was prepared from purified aqueous manganese sulfate solutions obtained from low grade Mn leach ore/residue containing 44 gdm^{-3} Mn and 22 gdm^{-3} H_2SO_4 at an anodic current density of 200 A m^{-2} in a glass cell. Purified $MnSO_4$ solution was obtained after leaching followed by two stages of purification of low grade Mn ore/residue.[9] The experimental set-up was outlined in our previous work.[7] Homologous surfactants SOS, SDS and STS (Fig. 1) were added at different concentrations into the electrolytic bath during electrolysis. EMD samples prepared from 0, 10 25, 50 and 100 mgL^{-1} of SOS, SDS and STS are labeled EMD_0, EMD_{SOS10}, EMD_{SOS25}, EMD_{SOS50}, EMD_{SOS100}, EMD_{SDS10}, EMD_{SDS25}, EMD_{SDS50}, EMD_{SDS100} and EMD_{STS10}, EMD_{STS25}, EMD_{STS50}, and EMD_{STS100} respectively. The anodic oxidation of Mn^{2+} to MnO_2 was carried out on a lead (Pb) anode placed in parallel to a stainless steel (SS) cathode. All experiments were carried out at around 90°C for 4 h. The dried mass of deposited material was ground and sieved through a 53-μm mesh to obtain EMD powder. The resultant product in powder form was washed repeatedly with deionized water until the sample was sulfate free. The EMD powder was finally dried and cooled in a desiccator and subject to physical and electrochemical characterization. Morphological characterization was performed on EMD flakes scraped from the anodes. These were washed with deionized water before analysis.

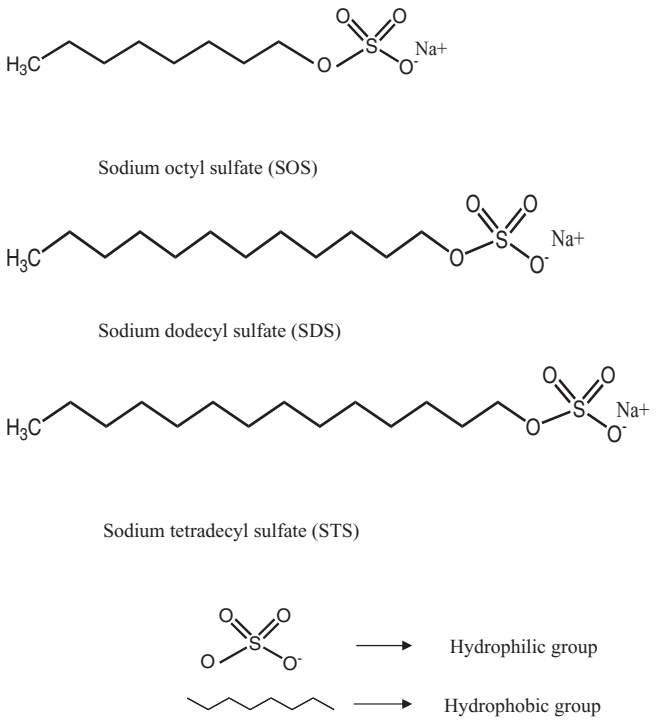

Figure 1. Molecular structures of the surfactants.

Physical characterization.— X-ray diffractograms were recorded for the EMD powders using PANalytical diffractometer (PW 1830, Philips, Japan) with Cu Kα radiation. The scans were recorded in the 2θ range 15–80°. The surface morphology of the EMD samples was determined using field emission scanning electron microscope (FESEM, ZEISS SUPRA 55). BET surface area and pore size analysis was carried out using Quantachrome (Autosorb-iQ) surface area analyzer. To measure the tap density, 2 g of each of the EMD samples was placed in a small graduated measuring cylinder and repeatedly tapped (200 times) using a tap density tester. The density of the powder showed a little change with the number of tappings, which was finally recorded as the tapping density of the powder. Fourier transform infrared (FT-IR) spectrographs were recorded on a Nicolet 6070 spectrophotometer in the frequency range 400–4500 cm^{-1}. Differential thermal analysis (DTA) and thermogravimetry (TG) (Perkin Elmer Diamond) analysis were carried out under inert atmosphere over a temperature range of 30 to 1000°C with a heating rate of 5 °C min^{-1}.

Electrochemical characterization.— The pellet preparation, cell arrangement and all other conditions and parameters remain as per previous reported work.[7] The EMD active material was first mixed with 20 wt% graphite powder and with 5 wt% polyvinyl alcohol as a binder and then pressed (pressure of 12 t) into a disc with a diameter of 20 mm. An electrochemical cell was constructed with the disc as the cathode, metallic Zn as the anode (equal mass to that of cathode). Initially, the cell assembly was allowed to equilibrate for 1 h at its open circuit voltage (OCV). The electrolyte was 9 M KOH. The applied discharge current was 20 mA (C/15 rate) with a cut-off voltage of 1.0 V. The applied charge current was 40 mA (C/7.5 rate) with a cut-off voltage of 1.6 V. The discharge capacities were recorded for up to 20 cycles. The galvanostatic measurements were carried out using a BITRODE deep cycle battery tester (LCN1-25-24, USA).

For cyclic voltammetric (CV) experiments, a standard three-electrode cell was used. For this purpose, EMD samples prepared in the presence of different concentrations of SOS, SDS and STS as anionic surfactants were used as the working electrode. The active material was pressed on to a disc of Pt gauze. On the other side of a disc, a layer of graphite powder was also pressed to enhance the conductivity. The MnO_2 side of a disc was exposed to the KOH electrolyte through a Teflon barrel. The exposed area was 0.5 cm in diameter. The counter electrode was a zinc foil, which was separated from the main electrolyte (9 M KOH) by means of a porous frit to avoid the spallation of zinc inserted into the MnO_2. Mercury-mercury oxide (Hg/HgO) served as the reference electrode. Reported potentials are relative to Hg/HgO. The working electrode was cycled between 0.2 and – 0.6 at 35 μV/s scan rate. On each occasion the potential scan started at 0.2 V, moving initially in the cathodic direction.

Results and Discussion

Electrolysis.— The electrochemical parameters, current efficiency (CE) and energy consumption (EC), of electrodeposited EMD prepared with and without surfactants are given in Table I. The surfactant free bath yields EMD with a CE of 94% and energy consumption of 1.640 kWh kg^{-1}, and with the introduction of surfactant the CE increases to a maximum level before decreasing on addition of excess of surfactant. The increase in CE suggests strong adsorption of the additives on the electrode surface.[24] It is worth noting that during EMD deposition at high temperature, hydrogen gas liberated at the cathode carries acidic mist to the air, which is hazardous to health and may cause damage to the environment, particularly at an industrial scale of EMD production.[32] Therefore an attempt has been made[33] to reduce the hydrogen evolution and the energy consumption by using a Pt/C gas diffusion electrode as the cathode during EMD production. Surfactant addition to the electrolytic bath causes formation of a froth which covers the solution interface and minimizes hydrogen evolution and the release of acid mist; this is thus an added advantage of the use of surfactant. The energy consumption also reduces to 1.353 kWh kg^{-1}

Table I. Effect of additives on the electrodeposition parameters of electrolytic manganese dioxide (EMD) from low grade Mn residue.

Surfactant	Additive conc. (mgL^{-1})	Current efficiency (%)	Energy Consumption ($kWhkg^{-1}$)	BET Surface area ($m^2\ g^{-1}$)
	Nil	94	1.640	100
SOS	10	99.5	1.370	107.001
	25	100	1.353	126.13
	50	98.5	1.446	115.917
	100	95	1.455	109.68
SDS	10	98	1.419	99.17
	25	92	1.583	115.679
	50	89	1.594	130.492
	100	88.8	1.598	94.54
STS	10	96	1.548	101.61
	25	96.5	1.540	124.529
	50	97.5	1.532	122.864
	100	93	1.590	103.29

at 25 ppm of SOS in the electrolyte against the energy consumption of 1.640 kWh kg^{-1} for surfactant free electrolyte.

In general, the electrodeposition of manganese dioxide[34] from an acidic sulfate solution proceeds through the following reactions:

$$\text{At Anode:} \quad Mn^{2+} + 2H_2O \rightarrow MnO_2 + 4H^+ + 2e^- \quad [1]$$

$$\text{At Cathode:} \quad 2H^+ + 2e^- \rightarrow H_2 \quad [2]$$

MnO_2 does not form at the anode in one single step. Initially Mn^{2+} is formed in solution and is converted to an intermediate species, Mn^{3+}, in its solid phase. This intermediate species finally gives rise to solid Mn^{4+} phase in the form of MnO_2 while some Mn^{2+} ions still remain in the solution phase.[35,36] When surfactants are present in solution, they may inhibit the formation of Mn^{3+} intermediate species in solution by adsorbing at the substrate/electrolytic solution interface. Surfactant molecules may also block active growth sites, thereby allowing electrodeposition preferentially on crevices.[37] The electron/ion transfer kinetics mostly depends on the degree of coverage of the electrode by surfactant due to either mechanical blocking or through electrostatic interactions.[38,39] Coverage of electrode with surfactant causes changes to the electrical double layer characteristics, which influence the interfacial energy, dielectric constant, potential and current distribution at the electrodes, ultimately resulting in modified crystal growth. Surfactants can significantly reduce surface tension and surface energy of nano-particles. The steric effect of long surfactant molecular chains can prevent them from agglomerating[28,40] hence, the organic surfactants play a crucial role in facilitating the formation of compact deposits with greater surface area. To the best of our knowledge, no systematic work has been done on the reported range of anionic surfactants and their dual role in promoting the material and electrochemical characteristics of the EMD material.

Structural characterization.— XRD patterns of EMD samples prepared at different concentrations of SOS, SDS and STS as anionic surfactants are shown in Fig. 2. All the EMD samples show weak, broad peaks indicating a small degree of crystallisation and a typical amorphous structure. The diffraction peaks can be indexed to an orthorhombic phase of γ-MnO_2 with lattice constants: $a = 8.70$ Å, $b = 2.90$ Å and $c = 4.41$ Å. These cell parameters are in good agreement with the standard values (JCPDS card no. 65–1298; $a = 9.27$ Å, $b = 2.87$ Å, $c = 4.53$ Å). The peaks at 2θ values of ∼22°, 37.2°, ∼42°, ∼56°, ∼68° correspond to the 110, 021, 121, 240/221, 002/061 crystal planes of γ-MnO_2, respectively. Addition of surfactant to the electrolytic bath had no significant effect on the crystalline phase of EMD.

Figure 3 shows the FTIR spectrum recorded for the EMD samples with or without surfactant at different frequency range. The peak

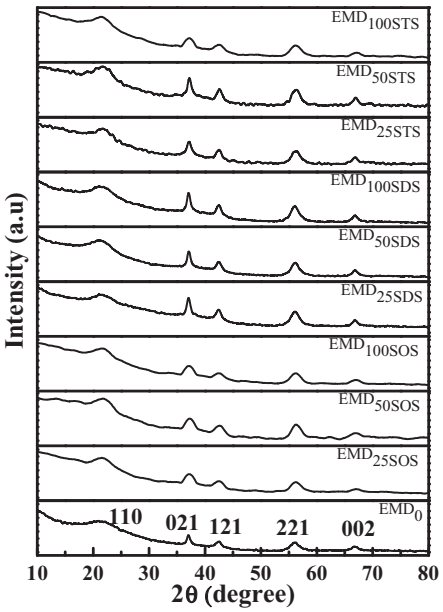

Figure 2. X-ray diffractogram of EMD samples.

detected in the finger print region of 400–600 cm^{-1} confirms the formation of γ-MnO_2. The broad peak located at about 760 cm^{-1} is assigned to the characteristic peak of MnO_6 octahedron, while the transmission band at 1100 cm^{-1} can be attributed to the MnO_2 stretching mode and/or O-H bending vibrations[41] associated with hydrogen bonding, indicating the presence of bound water molecules.[42,43] The strong band at ∼1630 cm^{-1} can be attributed to O-H bending vibrations associated with the water of crystallization[43] and a broad band at ∼3400 cm^{-1} is due to OH stretching vibrations.[42,43] A weak band is observed at ∼1400 cm^{-1} indicating O-H stretching vibrations.[44] FTIR data indicates that SOS, SDS and STS addition at the concentrations used in this study has no significant effect on EMD structure and composition. The absence of the characteristics peaks of the organic functional groups of the surfactants suggests that there is no residual surfactant present after the washing procedure.[43]

Surface morphology.— Addition of the surfactant during electrodeposition plays a vital role in modifying the structure of EMD by controlling the nucleation and growth mechanism through

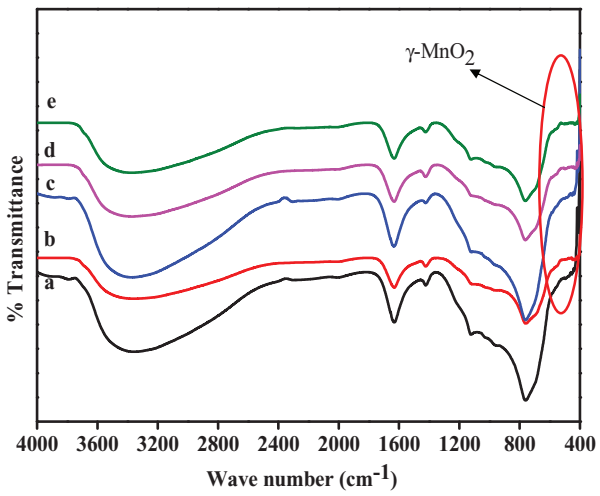

Figure 3. FTIR spectra of a) EMD_0, b) EMD_{SOS25}, C) EMD_{SDS50}, d) EMD_{STS25}, and e) EMD_{STS50}.

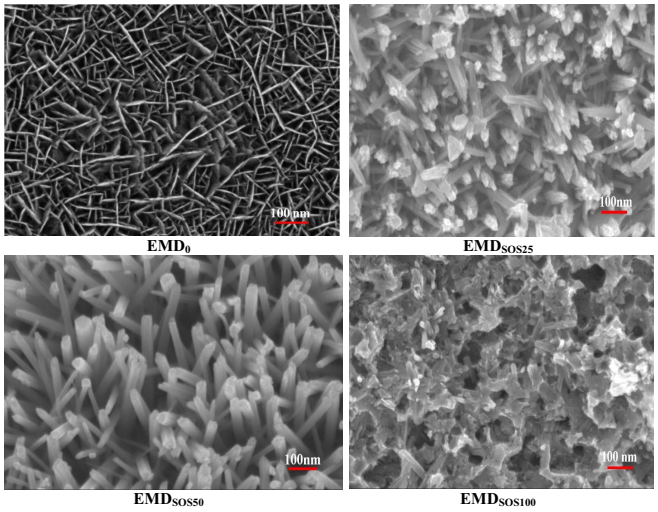

Figure 4. FESEM images of the EMD samples in the absence and presence of various concentrations of SOS as anionic surfactant.

adsorption, which in turn influences the stability and rechargeability of EMD.[24,45] Fig. 4 shows the FESEM images of the EMD samples. For EMD_0, particles exhibited platy growth oriented randomly in all directions relative to the axis perpendicular to the anode, forming a net-like deposit. In the presence of SOS tube-like particles with pointed and flat tip for EMD_{SOS25} and EMD_{SOS50} respectively are formed. With increasing SOS concentration (i.e, for EMD_{SOS100}), an irregular morphology of agglomerated particles with the occasional appearance of tube-like orientations was observed. When SDS was employed during electrosynthesis of EMD, a porous structure with narrow needle like particles was obtained for EMD_{SDS10} (Fig. 5a), however at 50 ppm concentration of SDS (i.e, for EMD_{SDS50}), narrow needle like particles within a size range of 50–100 nm were observed (Fig. 5b). EMD_{SDS100} showed (Fig. 5c) platy morphology with randomly oriented particles to produce a net-like appearance. Deposits obtained in the presence of STS shows quite different morphology (Fig. 5e–5f) than those obtained in the presence of SOS and SDS. EMD_{STS25} produced nano-sized rod-type grains with sizes in the range of 10–20 nm perpendicular to the anode surface, with some agglomeration evident. The EMD obtained in the presence of 50 ppm STS (EMD_{STS50}) consisted of nano-sized petal-like structures arranged in a random fashion, giving a highly porous structure, while the EMD obtained in the presence of 100 ppm STS (EMD_{STS100}) consisted of nano rods stacked at random. Thus the presence of all these anionic surfactants resulted in very highly porous nano materials.

BET surface area and porosity analysis.— Subsequent to FESEM studies, BET surface area analysis and pore size distribution studies were carried out by N_2 adsorption–desorption measurements to gain further insight into the structural behavior of EMD prepared in the presence and absence of anionic surfactants. The nitrogen adsorption–desorption isotherms are shown in Fig. 6a–6d. Both unmodified and modified EMD samples had typical type IV adsorption–desorption isotherms with H2 type hysteresis loops characteristic of mesoporous materials, with loop shifting to a higher relative pressure on approaching $P/P_0 = 1$, indicating a large number of mesopores. The isotherms agree well with the determined pore diameters of 4.172, 3.824, 3.836 and 3.817 nm for EMD_0, EMD_{SOS25}, EMD_{SDS50} and EMD_{STS25} respectively with corresponding pore volumes of 0.1385, 0.1105, 0.1311 and 0.1281 $cm^3\ g^{-1}$. The amount adsorbed gradually increased at lower relative pressures and then increased sharply at higher relative pressures. The pore size distribution curves (insets of Figs. 6a–6d) confirm that more intense peaks with ordered pores are formed in case of surfactant modified EMD samples. The BET surface areas of the EMD samples were found to be 100, 126.13, 130.492, 115.679 and 124.529 m^2/g for EMD_0, EMD_{SOS25}, EMD_{SDS25}, EMD_{SDS50} and EMD_{STS25} respectively, confirming the increase in surface area facilitated by the presence of surfactants. The tap densities for the EMD samples in the absence and presence of surfactant are found to be in the range of 1.8–2.0 and 2.4–2.8 g/cm^3 respectively. The high tap densities for surfactant assisted EMD are related to the porous structure with enhanced effective active sites for redox mechanism to occur.[46]

Thermal analysis.— Thermal analysis (TG and DTA) is an important tool to determine the structural stability of MnO_2 in terms of its water content, as water content in MnO_2 causes a variation in the crystal lattice, with consequent effects on electrical conductivity and electrode potential.[11] Among the three different types of water molecules associated with γ-MnO_2,[47] Type I water corresponding to physisorbed molecular water, is removed below 110°C. As observed in Fig. 7, there is greater weight loss in this region for surfactant modified EMD than the surfactant-free EMD, due to the higher surface area. Type II water, dissociatively chemisorbed water and strongly bound micropore water, is removed below 270°C. Type III water is present as hydroxyl groups in the interior of the lattice and is removed at around 300°C. The weight loss corresponding to these two types of water is comparatively less for surfactant-modified EMD samples than the unmodified samples. This is followed by the weight loss in the temperature ranges between 400–600 and 600–900°C, which may be attributed to the formation of Mn_2O_3 and Mn_3O_4, respectively.[48–50] The weight loss in the range of 400–600°C is more prominent for surfactant-free EMD than the surfactant modified EMD samples.

Figure 7b presents the DTA thermograms of the EMD samples. EMD_0 shows an endo peak below 100°C and a broad endo peak below 300°C, due to the continuous removal of types I, II, and III water. Note that the endo peak observed below 300°C for EMD_0 is less prominent in surfactant modified EMD samples. The sharp endo peak corresponding to the formation of Mn_2O_3 is prominent for surfactant-free EMD relative to the surfactant modified EMD samples. This in

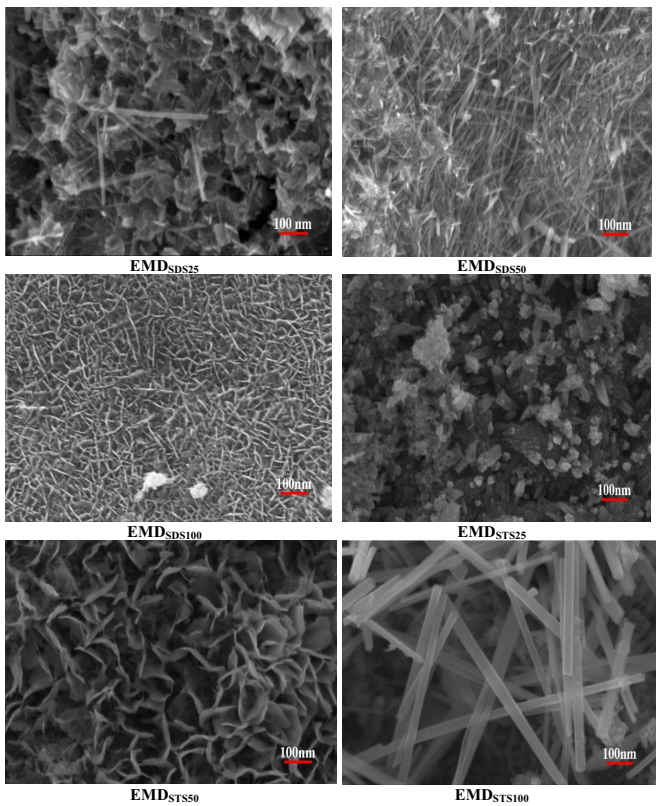

Figure 5. FESEM images of the EMD samples in the presence of various concentrations of SDS and STS as anionic surfactants.

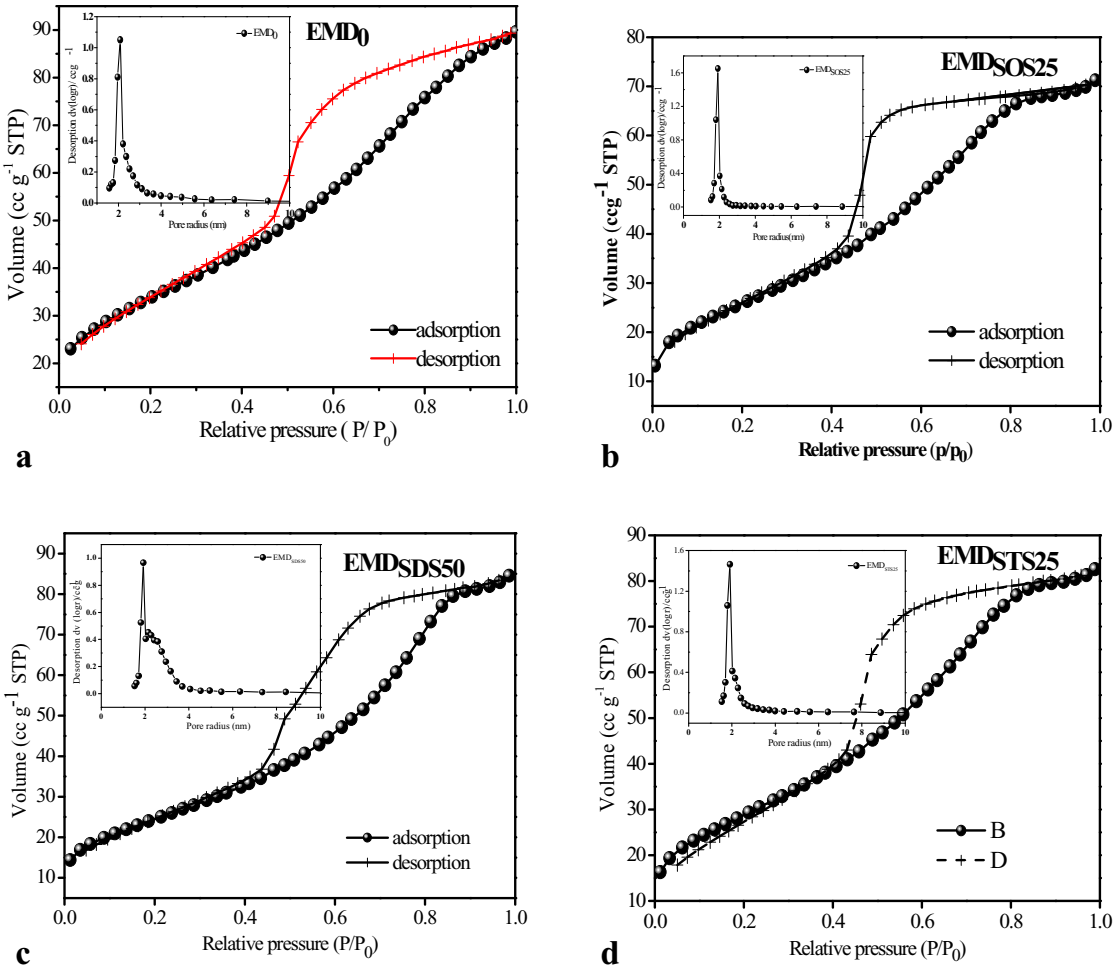

Figure 6. Nitrogen adsorption and desorption isotherm of EMD samples in the presence of various concentrations of anionic surfactants.

turn strongly supports the observation made by thermogravimetric analysis, indicating higher stability of the surfactant modified EMD samples when compared with unmodified one.

Electrochemical activity of EMD.— The electrochemical performance of the EMD samples was characterized both by galvanostatic (charge-discharge) and potentiostatic (cyclic voltammetry) techniques to identify suitability for energy storage applications. The galvanostatic technique involves the battery-type (charge – discharge) characteristics while imposing a constant current and evaluation of storage capability over a number of cycles. The EMD samples were subject to discharge first and were then charged in 9 M potassium hydroxide aqueous solutions. The redox processes that occur during charge-discharge have been discussed in our previous work.[10,29] The electrochemical reactions that takes place at the EMD electrode in aqueous electrolyte is the electron-proton mechanism corresponding to the insertion of H^+ accompanied by reduction of Mn sites (Mn^{4+} is reduced to Mn^{3+}) in MnO_2.[51]

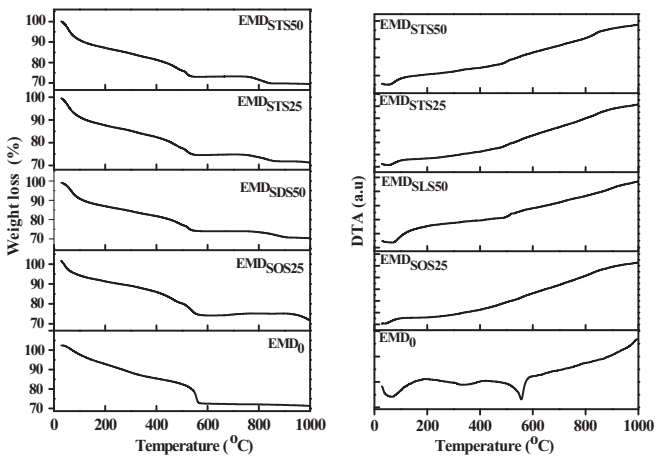

Figure 7. TG (left) and DTA (right) plots of EMD samples in the presence of various concentrations of anionic surfactants. Intensity of the y-axis is normalised.

The discharge behavior of EMD samples obtained with and without surfactants is shown in Fig. 8, 9 and 10. The discharge capacity of 267 $mAhg^{-1}$ was obtained for the surfactant-free EMD (EMD_0) against a reported discharge capacity of 160 $mAhg^{-1}$ in the absence of additives.[52] However, on continuous charge-discharge cycling the capacity faded gradually to a discharge capacity of 20 $mAhg^{-1}$ within 15 cycles, after which a sudden fall in discharge is observed due to capacity failure. The charge storage mechanism in MnO_2 is a single phase proton insertion originating from the water of the KOH electrolyte introduced into the ionic lattice of the MnO_2 corresponding to a redox process.[51] The structural irreversibility of MnO_2 during successive cycling is well reported in the literature.[51,53,54] The products of the materials produced after discharge are electrochemically inactive phases birnessite (δ-MnO_2), hausmannite (Mn_3O_4), and manganese oxy hydroxides ($Mn(OH)_2$).[54–56] These irreversible materials downgrade the cycleability of Zn-MnO_2 alkaline cells, while the presence of Bi- or Ba- containing compounds in the electrolyte suppresses the

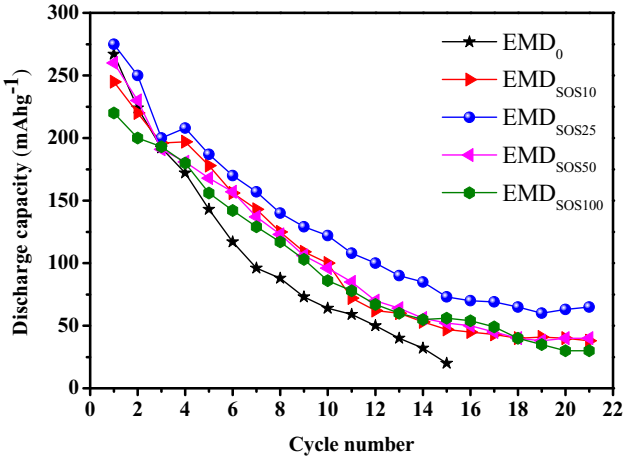

Figure 8. Discharge capacities versus cycling behavior of EMD at different concentration of SOS.

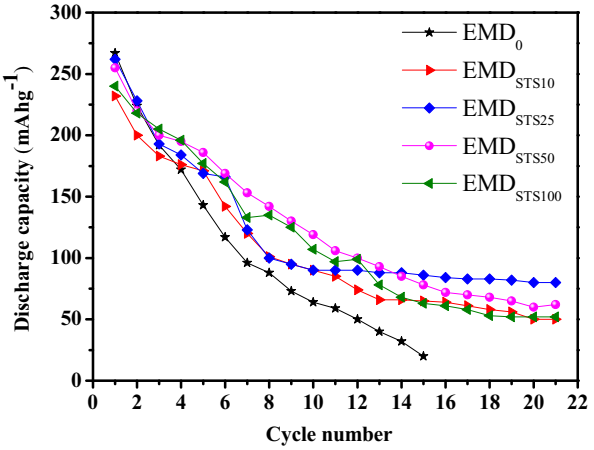

Figure 10. Discharge capacities versus cycling behavior of EMD at different concentration of STS.

formation of these materials.[55,56] However, this is outside the scope of this study. During the repeated cycling, the anodic Zn electrode, as well as the MnO_2 cathode, undergoes morphological changes, forming dendrites that limit the rechargeability after modest utilization.[57] The presence of ZnO and zincate complex ions, primarily $Zn(OH)_4^{2-}$ on the surface inhibit the MnO_2 reaction, promoting irreversible passivation, thereby lowering the attainable discharge capacity.[58]

EMD deposited in the presence of SOS at 25 ppm shows an initial discharge capacity of 275 $mAhg^{-1}$ with good cycling stability (Fig. 8), and more stable behavior beyond 15 cycles than EMD_0. The tube like crystal with pointed ends yields a higher surface area for EMD_{SOS25}, resulting in better rechargeability than EMD_0 with platy orientation and lesser surface area. EMD_{SOS50}, with its uniform tubular crystal orientation also provides better reversibility than EMD_0. Similarly EMD prepared in the presence of SDS at 50 ppm shows an initial discharge capacity of 265 $mAhg^{-1}$ and good cyclic stability, relative to EMD_0, with continuous charge-discharge cycling. EMD_{SDS50} shows a discharge capacity of 78 $mAhg^{-1}$ after 20 cycles (Fig. 9). This is due to the higher surface area for EMD_{SDS50} and the resultant nano needle like structures. However, EMD_{SDS50} shows gradual loss in discharge capacity with charge-discharge cycling due to higher concentration of surfactant resulting in lesser surface area with anisotropic crystal orientation.[59] The surfactant molecules in the electrolytic bath favor the adsorption process of Mn^{2+} ions at the electrode interface which precedes the redox process resulting in higher porous nature during the preparation of MnO_2. The electrodeposited MnO_2 in the presence of the surfactant possess high surface area relative to the material prepared in the absence of the surfactant. These surfactant molecules can form micelles that facilitate the insertion of protons into the MnO_2 moiety.[27] The presence of surfactants resulted in the formation of compact deposits, having larger surface area with improved particle to particle contact. EMD modified with STS shows the best cyclic stability at 25 ppm concentration. Although it shows an initial discharge capacity of 262 $mAhg^{-1}$, slightly lower than EMD_0, EMD_{STS25} interestingly shows the most stable cyclic behavior after 9th cycle onwards with discharge capacity of 95 $mAhg^{-1}$ (retaining 35% of the initial capacity) at the end of 20 cycles (Fig. 10). This may be due to the nano grain like morphology of EMD particles within the range of 10–100 nm. EMD_{STS50} also shows good cycling behavior, which may be attributed to the petal-shaped morphology. EMD samples with various concentration of several surfactants used in this study show better cyclic stability than the surfactant free EMD, indicating that these anionic surfactants influence the electrochemical activity of the EMD through a modification to morphology and a higher surface area. The adsorption seems to be larger in the presence of anionic surfactant (STS).[60] According to our physical and electrochemical studies, better deposition was obtained for EMD_{STS} as the surfactant with the optimal concentration (25–50 ppm). At higher concentration of surfactants (>50 ppm), the increase in interfacial viscosity resulted in irregular morphology comprising agglomerated nano-rod like structure. The major factor supporting the best performance of the capacity retention for EMD_{STS25} is related to the porous structure with regular crystal growth. This may influence the penetration of electrolyte into the voids and pores and eventually proton insertion within the MnO_2 lattice. This suggests that surface activity of a surfactant is proportional to its length of its tail group (Fig. 1) and inversely proportional to its critical micelle concentrations (CMC)[30] that governs the extent of its role and cycleability retention. To get a complete picture, discharge - charge characteristics for the cell Zn / EMD_{STS50} using 9M KOH as the electrolyte were investigated. The cell was galvanostatically discharged first and then charged. The results are shown in Fig. 11. During discharge, initially the voltage (1.6 V) dropped approximately to 1.55 V and then gradually decreased to the cut-off voltage of 1.0 V, equivalent to 265 mAh/g. On reversing the current, during the charge process, there was a steep increase in potential and then an inflection is seen at around 1.3 V. Finally, a plateau like curve is seen at 1.55 V before the cut-off voltage at 1.6 V. The cell is found to be reversibly charged with a coulombic efficiency of 91%. The voltage profiles for the other two surfactants (SOS and SDS) showed quite similar behavior without any significant difference in potential to that of STS.

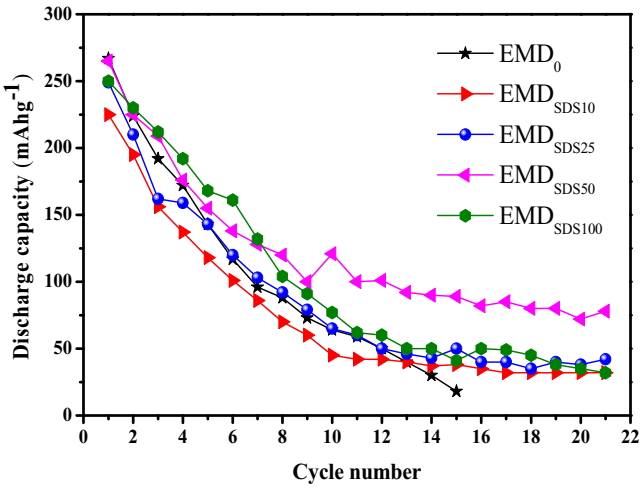

Figure 9. Discharge capacities versus cycling behavior of EMD at different concentration of SDS.

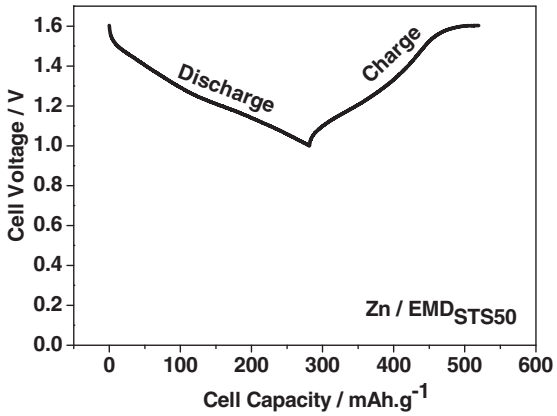

Figure 11. The first discharge - charge profile of Zn / EMD_{STS50} cell using 9M KOH electrolyte.

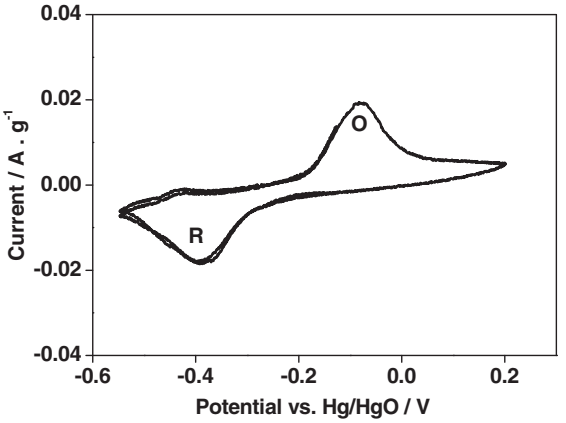

Figure 12. Cyclic voltammogram of surfactant free EMD sample, potential scanned at a scan rate of 35 μV/s.

Figures 12–15 show typical cyclic voltammograms of EMD samples in the absence and presence of surfactants. The scan was initiated at 0.3 V moving in the cathodic (reduction) direction to –0.6 V and then reversing it back to the starting potential through anodic (oxidation) process. A pair of reduction (R at –0.41 V) and oxidation (O at 0.002 V) peaks have been identified, corresponding to $Mn^{4+/3+}$ redox ions,[61] for all the scans irrespective of the type and concentration of surfactant used. However, the peaks are ill defined for the higher concentration (100 ppm) of all surfactants used, (Figs. 13d, 14d, and 15d) suggesting an adverse effect on the MnO_2 crystal structure. For the surfactant free EMD (Fig. 11), and the lower concentration of surfactant (10 ppm) (Figs. 13a, 14a, and 15a), the areas under the peak are significantly less, implying the electrodeposited material lacking morphology inhibits the trafficking of ions from the electrolyte.[62] The EMD prepared in the presence of surfactant at concentrations of 25 and 50 ppm show well-defined redox peaks. Among all the surfactants studied, sodium tetradecyl sulfate (STS) shows cycling stability and peaks increasingly defined peaks on multiple cycles. The electrochemical studies suggest that the EMD material undergoes electro-reduction and oxidation in aqueous KOH electrolyte with an improved storage capability for STS as the surfactant. The optimum concentration of surfactant was found to be between 25 and 50 ppm in the electrolytic bath during electrolysis.

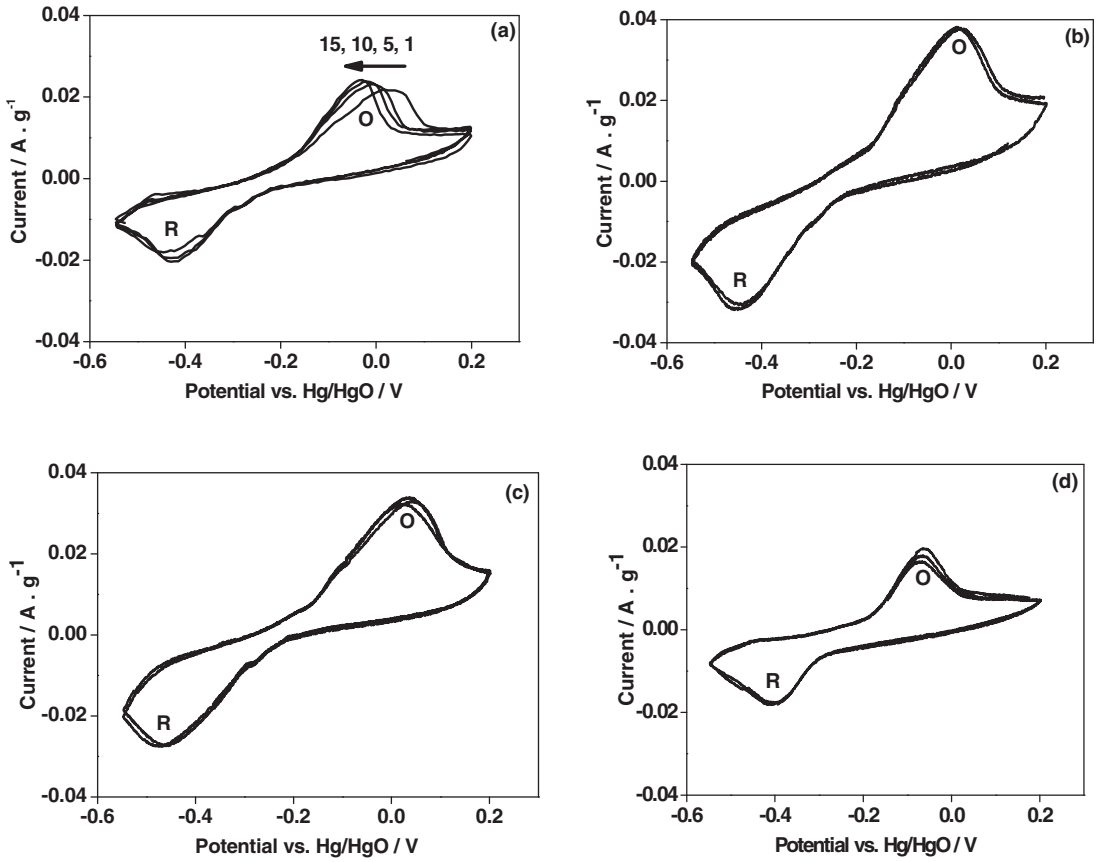

Figure 13. Cyclic voltammogram of EMD samples at different concentrations of SOS (a) 10, (b) 25, (c) 50 and (d) 100 ppm, potential scanned at a scan rate of 35 μV/s. Cycle numbers are indicated in the figure. The term "R" and "O" denotes reduction and oxidation respectively.

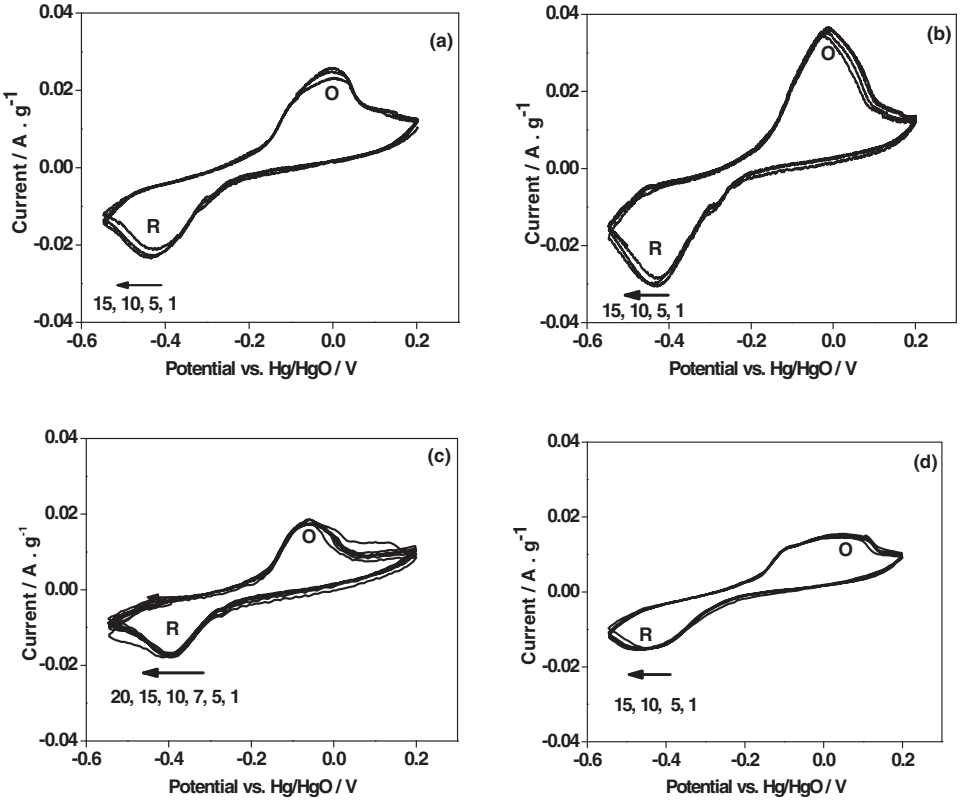

Figure 14. Cyclic voltammogram of EMD samples at different concentrations of SDS (a) 10, (b) 25, (c) 50 and (d) 100 ppm, potential scanned at a scan rate of 35 μV/s. Cycle numbers are indicated in the figure. The term "R" and "O" denotes reduction and oxidation respectively.

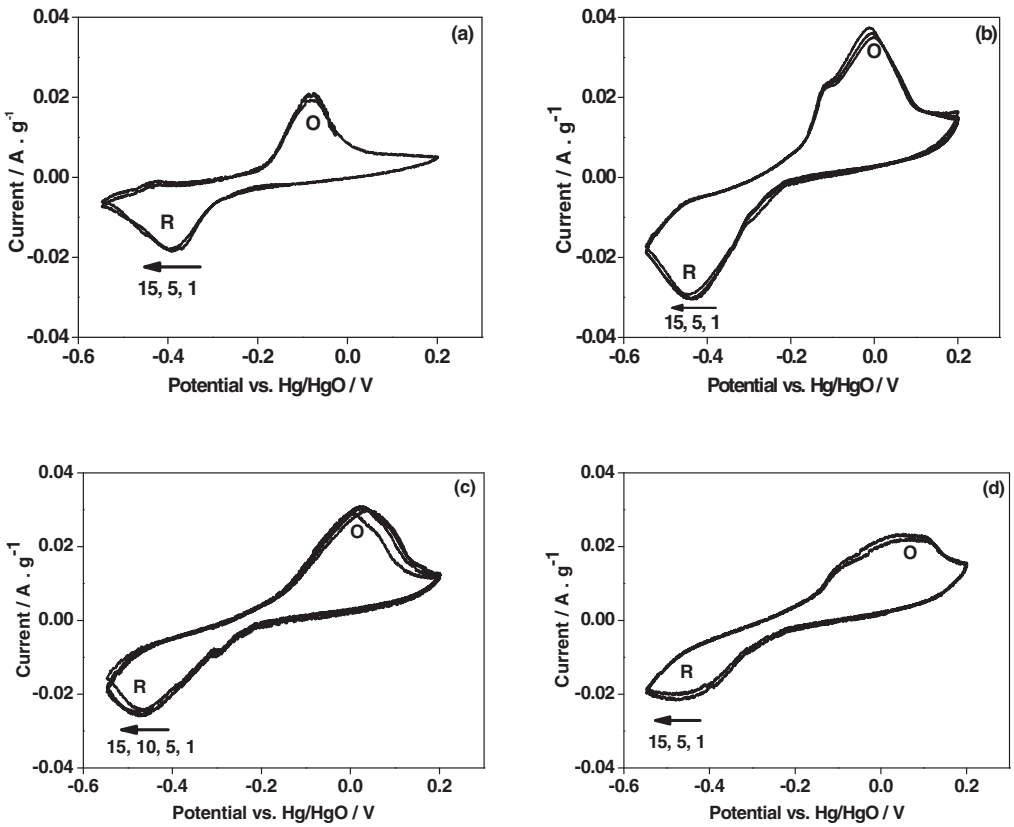

Figure 15. Cyclic voltammogram of EMD samples at different concentrations of STS (a) 10, (b) 25, (c) 50 and (d) 100 ppm, potential scanned at a scan rate of 35 μV/s. Cycle numbers are indicated in the figure. The term "R" and "O" denotes reduction and oxidation respectively.

Conclusions

All the anionic surfactants influenced EMD crystal morphology. Efficiency and energy consumption depends on the type and concentration of surfactant used. The morphology of the electrodeposited manganese dioxide (EMD) particles, in the absence and presence of anionic surfactants, showed preferential adsorption of a surfactant will delay the relative growth rates of MnO_2 particles. The presence of sodium tetradecyl sulfate (STS) as surfactant during EMD deposition efficiently promotes both ion and electron transport in the host MnO_2 matrix due to its nanostructured deposition, forming a highly porous structure. Electrochemical studies of the electrodeposited EMD in the presence of STS as a surfactant indicate it is a potential candidate for use as electrode material in alkaline rechargeable batteries. The dual role of surfactant, assisted in having nano aggregate particles and trafficking the redox ions from the electrolyte to the host compound while retaining the 35% of the initial discharge capacity after multiple cycles. In the case of surfactant free EMD the capacity retention was just 7% after multiple cycles.

Acknowledgments

The authors are thankful to Prof. B.K Mishra, Director, CSIR-IMMT, Bhubaneswar, for permission to publish the paper. Authors also thank the Ministry of Earth Sciences, Govt. of India for partly sponsoring the work. The first author, A. Biswal is thankful to Council of Scientific and Industrial Research (CSIR), India for awarding Senior Research Fellowship. The author (M.M.) wishes to thank the Australian Research Council (ARC). Authors from Murdoch University wishes to acknowledge the receipt of SEIT seed grant through which part of the work has been generated.

References

1. U. Kohler, C. Antonius, and P. Bauerlein, *J. Power Sources* **127**, 45 (2004).
2. W. J. Wruck, B. Reichman, K. R. Bullock, and W.-H. Koo, *J. Electrochem. Soc.* **138**, 3560 (1991).
3. Y. Morioka, S. Narukawa, and T. Itou, *J. Power Sources* **100**, 107 (2001).
4. F. Beck and P. Ruetschi, *Electrochim. Acta* **45**, 2467 (2000).
5. W. Zhang and C. Y. Cheng, *Hydrometallurgy* **89**, 137 (2007).
6. A. Biswal, K. Sanjay, M. K. Ghosh, T. Subbaiah, and B. K. Mishra, *Hydrometallurgy* **110**, 44 (2011).
7. A. Biswal, B. C. Tripathy, T. Subbaiah, D. Meyrick, and M. Minakshi, *J. Solid State Electrochem.* **17**, 3191 (2013).
8. A. Biswal, B. Dash, B. C. Tripathy, T. Subbaiah, S. M. Shin, K. Sanjay, and B. K. Mishra, *Hydrometallurgy* **140**, 151 (2013).
9. A. Biswal, B. Nayak, B. Dash, K. Sanjay, T. Subbaiah, and B. K. Mishra, *Eur. Metall. Conf.* **4**, 1323 (2011).
10. N. K. Mittal and P. K. Sen, *Minerals Engineering* **16**, 865 (2003).
11. S. C. Pang, M. A. Anderson, and T. W. Chapman, *J. Electrochem. Soc.* **147**, 444 (2000).
12. J. P. Rethinaraj and S. Visvanathan, *J. Power Sources* **42**, 335 (1993).
13. Y. Shen and K. Kordesch, *J. Power Sources* **87**, 162 (2000).
14. Y. Sharma, M. Aziz, J. Yusof, and K. Kordesch, *J. Power Sources* **94**, 129 (2001).
15. W. Jantscher, L. Binder, D. A. Fielder, R. Andreaus, and K. Kordesch, *J. Power Sources* **79**, 9 (1999).
16. X. Zhao, L. Ma, and X. Shen, *J. Mater. Chem.* **22**, 277 (2012).
17. A. Urfer, G. A. Lawrance, and D. A. J. Swinkels, *J. Appl. Electrochem.* **27**, 667 (1997).
18. K. Kordesch and M. Weissenbacher, *J. Power Sources* **51**, 61 (1994).
19. S. Chou, F. Cheng, and J. Chen, *J. Power Sources* **162**, 727 (2006).
20. Y. Li, H. Xie, J. Wang, and L. Chen, *Mater. Lett.* **65**, 403 (2011).
21. R. Jiang, T. Huang, J. Liu, J. Zhuang, and A. Yu, *Electrochim. Acta* **54**, 3047 (2009).
22. H. Zhang, Y. Wang, C. Liu, and H. Jiang, *J. Alloys and Compds.* **517**, 1 (2012).
23. T. Zhao, H. Jiang, and J. Ma, *J. Power Sources* **196**, 860 (2011).
24. M. Ghaemi, L. K. Fard, and J. Neshati, *J. Power Sources* **141**, 340 (2005).
25. B. Prelot, F. Villieras, M. Pelletier, A. Razafitianamaharavo, F. Thomas, and C. Poinsignon, *J. Colloidal and Interface Sci.* **264**, 343 (2003).
26. A. Biswal, B. C. Tripathy, T. Subbaiah, D. Meyrick, and M. Minakshi, *J. Solid State Electrochem.* **17**, 1349 (2013).
27. B. Suhasini, *J. Electroanal. Chem.* **690**, 13 (2013).
28. H. Zhang, J. Gu, Y. Jiang, J. Zhao, X. Zhang, and C. Wang, *J. Solid State Electrochem.* **18**, 235 (2014).
29. A. Biswal, B. C. Tripathy, T. Subbaiah, D. Meyrick, M. Ionescu, and M. Minakshi, *Metallur. and Mater. Trans. E* **1**, 226 (2014).
30. V. Kumar and C. A. Steiner, *Colloids and Surfaces A: Physicochemical and Engineering Aspects* **147**, 27 (1999).
31. P. Mukerjee and K. J. Mysels, Critical Micelle Concentrations of Aqueous Surfactant Systems, National Standard Reference Series, National Bureau of Standards, Washington DC, (1971) p. 51–53, 115–122.
32. R. Al Shakarji, Y. He, and S. Gregory, *Hydrometallurgy* **131–132**, 76 (2013).
33. J. Tang, H. M. Meng, and L. L. Huang, *RSC Adv.* **4**, 16512 (2014).
34. J. Gong and G. Zangari, *J. Electrochem. Soc.* **149**, C209 (2002).
35. S. Nijjer, J. Thonstad, and G. M. Haarberg, *Electrochim. Acta* **46**, 395 (2000).
36. W. H. Kao and V. J. Weibel, *J. Appl. Electrochem.* **22**, 21 (1992).
37. K. Boto, *Electrodeposition and Sur. Treatment* **3**, 77 (1975).
38. Z. Kozarac, S. Nikolic, and B. Cosovic, *J. Electroanal. Chem.* **137**, 279 (1982).
39. I. Felhosi, J. Telegdi, G. Palinkas, and E. Kalman, *Electrochim. Acta* **47**, 2335 (2002).
40. M. Nakayama, M. Shamoto, and A. Kamimura, *Chem. Mater.* **22**, 5887 (2010).
41. H. Abbas and S. A. Nasser, *J. Power Sources* **58**, 15 (1996).
42. M. V. Ananth, S. Pethkar, and K. Dakshinamurthi, *J. Power Sources* **75**, 278 (1998).
43. J. B. Fernandes, B. Desai, and V. N. Kamat Dalal, *Electrochim. Acta* **28**, 309 (1983).
44. J. Fitzpatrick, L. A. H. Maclean, D. A. J. Swinkels, and F. L. Tye, *J. Appl. Electrochem.* **27**, 243 (1997).
45. J. O. Besenhard, J. Gurtler, P. Komenda, and A. Paxinos, *J. Power Sources* **20**, 253 (1987).
46. M.-Y. Cho, H. Kim, H. Kim, Y. S. Lim, K.-B. Kim, J.-W. Lee, K. Kang, and K. C. Roh, *J. Mater. Chem. A* **2**, 5922 (2014).
47. J. A. Lee, C. E. Newman, F. S. Stone, and F. L. Tye, *J. Colloid and Interface Sci.* **45**, 289 (1973).
48. J. H. Sharp and D. M. Tinsley, *J. Therm. Anal.* **3**, 43 (1971).
49. J. P. Brenet and P. Faber, Symp. I. S. E. Batteries Marcoussis, France (1995).
50. J. B. Fernandes, B. Desai, and V. N. Kamat Dalal, *Electrochim. Acta* **29**, 187 (1984).
51. K. Kordesch, J. Gsellmann, M. Peri, K. Tomantschger, and R. Chemelli, *Electrochim. Acta* **26**, 1495 (1981).
52. M. M. Thackeray, *Progress in Solid State Chem.* **25**, 1 (1997).
53. C. Mondolini, M. Laborde, J. Dioux, E. Andoni, and C. Levy-Clement, *J. Electrochem. Soc.* **139**, 954 (1992).
54. F. L. Tye, *Electrochim. Acta* **30**, 17 (1985).
55. H. S. Wroblowa and N. Gupta, *J. Electroanal. Chem.* **238**, 93 (1987).
56. D. Im and A. Manthiram, *J. Electrochem. Soc.* **150**, A68 (2003).
57. J. W. Gallaway, C. K. Erdonmez, Z. Zhong, M. Croft, L. A. Sviridov, T. Z. Sholklapper, D. E. Turney, S. Banerjee, and D. A. Steingart, *J. Mater. Chem. A* **2**, 2757 (2014).
58. M. Minakshi, D. Appadoo, and D. E. Martin, *Electrochem. Solid State Lett.* **13**, A77 (2010).
59. S. Devaraj and N. Munichandraiah, *Electrochem. Solid State Lett.* **8**, A373 (2005).
60. E. Grzadka, *Cellulose* **20**, 1313 (2013).
61. M. Minakshi, P. Singh, T. B. Issa, S. Thurgate, and R. De Marco, *J. Power Sources* **153**, 165 (2006).
62. D. K. Walanda, G. A. Lawrance, and S. W. Donne, *J. Power Sources* **139**, 325 (2005).